Stretchable Electromagnetic Actuators for Underwater Soft Robots

Zhengxu Tang*[1,2], Yunnuo Zhang*[1,3], Abdallah Daha[1], Liuxi Xing[1], Vittorio Mottini[1], and Jinxing Li[1,4]

***Abstract*— Leveraging their intrinsically flexible and stretchable nature granted by the choice of soft materials, soft robots allow the development of more adaptive robotics systems in various environments. The electromagnetic actuator is a promising actuating modality to make flexible actuators. However, most of the electromagnetic actuators are made of metallic materials with limited softness and stretchability. In this work, we introduce a novel fabrication method of soft electromagnetic actuators (SEMAs) with highly stretchable conductive silver composite coils encapsulated with elastomers. We discuss the actuation mechanism, matter-of-hour fabrication process, ultra-thin property, low power consumption, and stretchable mechanical properties as well as soft robotic system designs enabled by the SEMAs. The SEMAs exhibit a stretchability of near 100% with good conductivity. Powered by an external amplifier with lower than 20V, the preliminary test on the illustrative soft robot demonstrates a movement speed of around 0.3 body length per second, as well as a soft, deformable, and stretchable nature of the movement. Our tunable SEMAs also demonstrate the potential for untethered, autonomous underwater soft robots and an infinite degree of freedom of movement with a programmable external magnetic field.**

I. INTRODUCTION

The escalating complexity of robotic operating environments has ushered in the rise of soft robotics as an important research field [1]-[4]. As a result, hydraulic and pneumatic actuation, dielectric elastomers, carbon nanotubes, polymer fibers, and shape-memory liquid crystal elastomers have been extensively explored and demonstrated for a wide range of applications[5]-[9]. However, many of these actuation mechanisms inevitably raise the requirement for an external infrastructure to provide support to functionalities, such as high voltages, and the existence of such infrastructures creates pertinent challenges in integrating them into soft robot designs, especially when operating in close proximity to humans or in intricate environments such as underwater.

Of the existing designs of soft actuators, electromagnetic actuators convert electrical energy into a variable magnetic field. They can not only provide a theoretically infinite degree of freedom but also require a very low energy density in powering the device, and thus an efficient transformation from energy storage to the desired kinetic energy[10], [11]. Electromagnetic actuation also has the advantages of low-voltage operation, easy integration, and miniaturization. Although the electromagnet actuators provide flexible actuation, they are still made of rigid metallic and plastic substrates, which limits their deformability and stretchability. Therefore, it is essential to explore new materials and designs that can make highly soft and stretchable actuators that can mimic biological systems with highly stretchable actuators.

Our goal in this work, therefore, was to provide a novel insight into fabricating stretchable, miniature, and biocompatible (in terms of driving voltage) SEMAs that are capable of performing actuation tasks in both air and water. Using a microfabricated highly stretchable silver composite

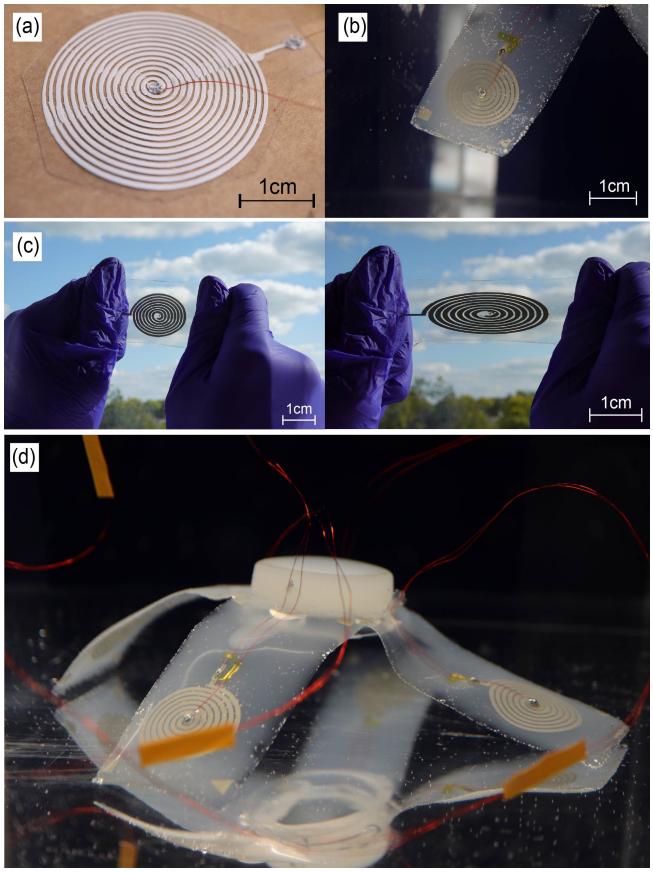

Fig. 1. Overview of the soft electromagnetic actuator and the proof-of-concept underwater soft robot. (a-b). A detailed look at the screen-printed Ag-based electromagnetic actuator (a) in air and (b) underwater. (c) Photos showing the highly soft and stretchable electromagnetic actuator. (d) The assembly of the untethered robotic octopus with four legs of an individual electromagnetic actuator.

*These authors contributed equally to the work

[1]Z. Tang, V. Mottini, Y. Zhang, A. Daha, L. Xing, and J. Li are with the Institute for Quantitative Health Science & Engineering, Michigan State University, East Lansing, MI, USA. (Corresponding author: J. Li jl@msu.edu)

[2]Z. Tang is also with the College of Literature, Science, and the Arts, University of Michigan, Ann Arbor, MI, USA

[3]Y. Zhang is also with the School of Interactive Computing, Georgia Institute of Technology, Atlanta, GA, USA

[4]J. Li is also with the Department of Electrical and Computer Engineering, Department of Chemical Engineering and Materials Science, Neuroscience Program, and Cell & Molecular Biology Program, Michigan State University, East Lansing, MI, USA.

ink, we are able to make soft and stretchable electromagnetic actuators with a low modulus of human skin, and a stretchability of nearly 100%. The designed fabrication process is not only straightforward but also time-efficient, where the sealing process can also be integrated seamlessly to enable actuation underwater. Integrating multiple SEMAs leads to an octopus-like soft robot that can be powered with a voltage of 20V, an operation frequency of around 1Hz, and a maximum traction speed of 0.3 body lengths per second. Detailed designs and fabrication processes are discussed in section III. We also present an illustrative design of an underwater soft robot powered by our soft electromagnetic actuator in section IV.

II. RELATED WORK

Various designs of soft actuators with different propelling mechanisms have been proposed in previous studies. Yet, contemporary designs of functional soft actuators are not without limitations. Hydraulic and pneumatic actuators, as mentioned in the introduction section, have dominated wide use in soft robotics due to their high-power output. However, they have strict requirements on the infrastructure used for their need for high-pressures (up to 300kPa) [7], [9]. Moreover, they usually have a very slow response speed (below 1 Hz) [12], making them more suitable for tethered tasks such as gripping or even rehabilitation instead of locomotion [12], [13]. Dielectric elastomer actuators (DEA) are among the most popular choices of material for the control of soft robots due to their outstanding mechanical properties as well as their softness and high traveling speed[14]-[17]. However, actuation of such elastomer would usually require up to thousands of voltages. This necessitates an extra layer of fabrication complexity in integrating high-voltage boost converters, introducing additional system intricacies and potential safety concerns. The integration of ferromagnetic fillers in elastomers is another promising solution, which not only miniaturizes and frees the system from tethers but also facilitates a safer, more wireless manipulation of soft robots[18], [19]. However, not only does the fabrication complexity remain, they are still not ideal as they usually require a careful design for only a set of pre-designed movements, whereas, in a real-world setting, the optimal movement of soft robots anticipates a high degree of post-production autonomous movement flexibility.

Therefore, electromagnetic actuators, constructed with 2-D or 3-D spiral shape coils with different materials and driven by interaction with external magnets, offer promise for advancing soft robot locomotion. Electromagnetic actuators offer various advantages in both tethered and untethered actuation compared to other designs for their high degree of freedom and low power consumption[10], [11], [23]. Previous studies on electromagnetic actuators mostly focused on spirals with conductive metals, which often need strict laboratory techniques such as Micro-electromechanical systems (MEMS) for fabrication [22], [23], or rigid 3-D spirals with huge sizes for high-frequency flapping or oscillation [24]. Investigations on 2-D SEMAs are relatively novel and unstudied, despite the earliest development of electromagnetic systems can be traced back to 1988 [25]. One of the major limitations in developing a 2-D SEMA is the choice of a highly stretchable and conductive material.

Prior studies by Mao et al. have established that electromagnetic actuators employing liquid metal coils excel in underwater soft robot actuation and interactions with everyday objects [20]. Likewise, Rogers et al. illustrate a whole network driven by liquid-metal-based electromagnetic actuators that are capable of doing rapid transformations of 3-D structures [28]. However, the inherent complexities in liquid metal-based SEMA fabrication, which involves processes like molding, airbrushing, or bolding, present challenges. Additionally, the necessary elastomer encasing and encapsulating the liquid metal is often thick, imposing limitations on the actuator's flexibility and functionality due to increased rigidity and weight[17], [18], [28].

The recent rise of soft electronics enabled many materials with great conductivity and stretchability [29], [30]. Our recent work shows that conductive silver ink can be developed to make highly soft and stretchable RFID tags [31]. In this work, for the first time, we engineer such a highly stretchable silver-based conductor with a direct printing process to develop soft electromagnetic actuators to make stretchable soft robots. Our actuator differs and outstands existing bodies of work in soft actuators because (i) it is extremely thin (less than 0.25mm) and light (less than 0.1g) as compared to [10],[20]; (ii) a lower power requirement (up to 20V) as opposed to soft actuators fabricated with other materials like dielectric elastomers (up to 10kV) [14]-[17]; (iii)being modular and independent of the modular body and shows capability in performing autonomous movements compare to [18], [19]; (iv)with-in-hour fabrication process that eliminates the need for molding and injecting, and customizable shape and substrate choice, as opposed to [20], [21]. Moreover, we present a proof-of-concept design inspired by an octopus, exhibiting remarkable underwater agility in complex underwater maneuvers, as well as a safe and easy sealing process to ensure successful underwater operations. While each actuator in our design is currently tethered and powered by a distinct signal generator, our findings highlight the potential for future untethered designs with integrated power systems. We will provide detailed working principles, fabrication processes, and experiment results in the following sections.

III. ACTUATOR DESIGN

A. Working Principle

As depicted in Fig. 2, depending on the different positions of the permanent magnet, the SEMA is driven by two different mechanisms. Fig. 2(b) describes the case when the permanent magnet is present below the actuator, generating a homogenous magnetic field parallel to the direction where the actuator is hung. In this scenario, the actuation is mainly driven by the Lorentz force on the moving charges of the SEMA. The force is calculated according to the standard Lorentz force law:

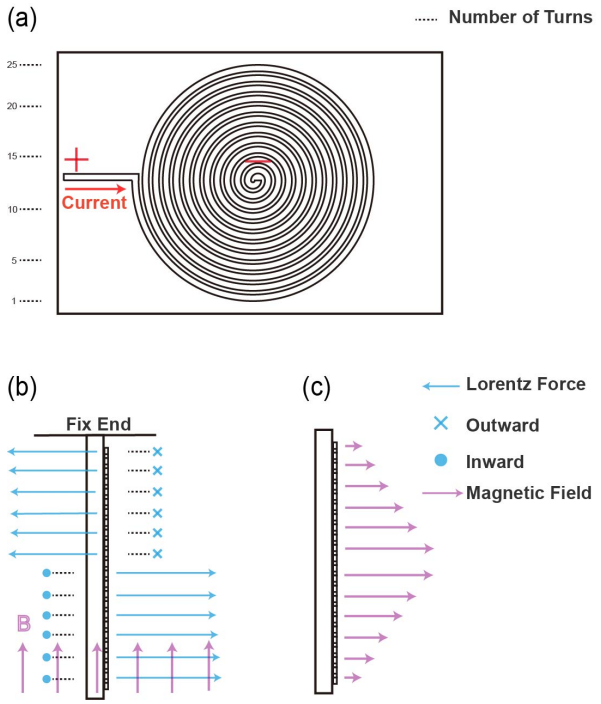

Fig. 2. Working principle of electromagnetic actuators. (a). A general schematic of the SEMA (b). A permanent magnet is placed below the SEMA, leading to actuation by Lorentz force. (c). The magnetic field is generated as described in the Ampere-Maxwell equation.

$$F = I \int dl \times B \tag{1}$$

where I indicates the current passing through the wire, dl indicates an infinitesimal segment of the SEMA, and B is an external magnetic flux provided by a permanent magnet. Depending on the current direction, the direction of the Lorentz force acting on the SEMA changes accordingly. Theoretically, with a uniform distribution of the current amplitude as well as a homogenous magnetic field over the SEMA, the Lorentz acting on different parts of SEMA should be the same. However, in real-world scenarios, a fix-end is applied during the experiment. This makes the Lorentz force applied on the lower part have a greater lever arm, and thus greater torque in actuating the SEMA.

Fig. 2(c) describes the case when the permanent magnet is present parallel to the SEMA, treating the SEMA as another permanent magnet. In this case, the magnetic field generated by a single loop inside the SEMA can be described as:

$$\vec{B}(r) = \frac{\mu_0}{4\pi} \int_C IdI \times \frac{r\prime}{|r\prime|^3} \tag{2}$$

Where C enclosed a loop path of any given circles with radius R inside the SEMA, μ_0 is the space permeability constant, I is the current amplitude, and $r\prime$ is the displacement vector between the evaluated point p and the infinitesimal current element IdI on the SEMA[27]. For a SEMA with specific current I, equation (2) can have a semi-analytical solution at any point in the direction depicted in Fig. 2(c):

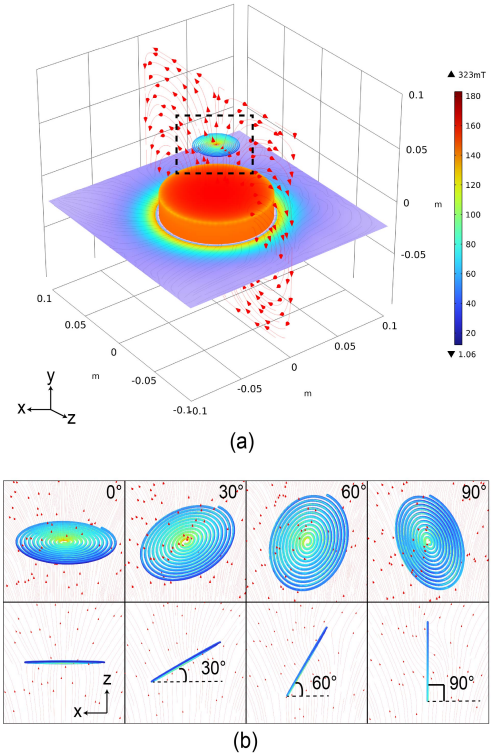

Fig. 3. The simulation result of the magnetic field distribution. (a) The magnetic field is generated by the coil and permanent magnet. The voltage applied on the coil is the maximum value of 20 V. (b) Characterization of the ambient magnetic field of the coil as the angle between the coil and the magnet changes.

$$B_x^j = \sum_{i=1}^{n} \frac{Cxz}{2\alpha^2\beta\rho^2}[(x_i'^2 + r^2)E(k^2) - a^2K(k^2)]$$

$$B_y^j = \sum_{i=1}^{n} \frac{Cyz}{2\alpha^2\beta\rho^2}[(x_i'^2 + r^2)E(k^2) - a^2K(k^2)]$$

$$B_z^j = \sum_{i=1}^{n} \frac{C}{2\alpha^2\beta}[(x_i'^2 - r^2)E(k^2) + a^2K(k^2)] \tag{3}$$

where $C = \mu_0 I/\pi$, $r^2 = x^2+y^2+z^2$, $\rho^2 = x^2+y^2$, $a^2 = x_i'^2 + r^3 - 2x_i'\rho$, $\beta^2 = x_i'^2 + r^2 + 2x_i'\rho$, and $k^2 = 1 - \alpha^2/\beta^2$ [27]. In this case, the Lorentz force on the moving charges of the SEMA is parallel to the direction of the SEMA being hung, generating a force directing downward as depicted in Fig 2(c), and thus does not help with the actuation.

To characterize the generated magnetic field to identify the interaction between the permanent magnet and SEMA, the spatial magnetic field distribution of a SEMA and an underneath magnetic cylinder (N52 Nd-Fe-B, D=100 mm, h=20 mm) is simulated in COMSOL Multiphysics. Fig. 3 (a) shows the magnetic distribution when the coil is parallel to the orientation direction of the magnetic cube, the magnetic lines and arrows show the symmetrical distribution of the system. When the cross-angle changes from 0°to 90°, the

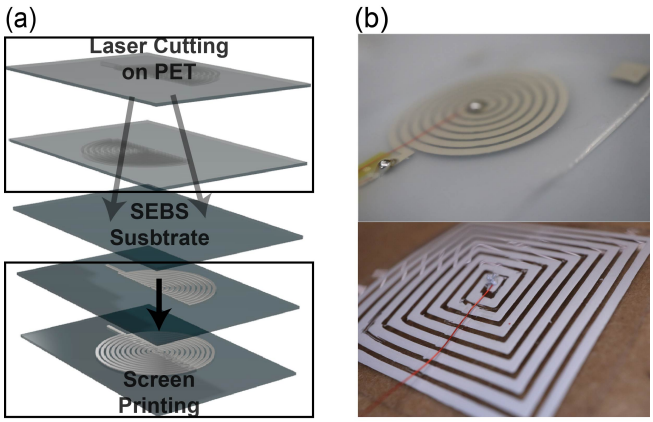

Fig. 4. Fabrication process of the electromagnetic actuator. (a). An exploded view of the fabrication. The PET film is separated into the upper part and lower part to prevent potential crosslinks of the circuit during the screen printing process. (b). Close-up shot of fine details of different shapes of SEMA upon fabrication.

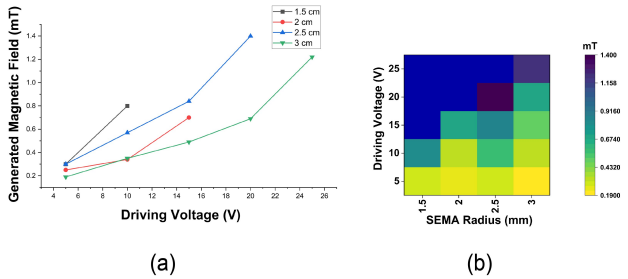

Fig. 5. Relation between different sizes of spiral and their corresponding magnetic field generated under different driving voltages. (a). Graph showing a negative correlation between the magnetic field generated and the size of the SEMA. (b). A heat map showing the strength of the magnetic field generated by different SEMAs, indicating an optimal design at a radius of 2.5cm

magnetic fields surrounding the coils are shown in Fig. 3 (b), representing the two boundary conditions of the coil motion.

IV. FABRICATION PROCESS

A. Fabrication of Individual Electromagnetic Actuator

One of the main goals of this study is to achieve an easy fabrication process. As shown in Fig. 3, the SEMA is fabricated through a standard screen printing process. The substrate is prepared by drop-casting or spin-coating SEBS (Asahi Kasei Tuftec ™1062, 0.15 g/mL mixed with cyclohexane or acetone) solution onto glass slides and waiting until the end of the solvent evaporation process. After laser patterning the SEMA shape (VLS6.60 Laser System, UNIVERSAL LASER SYSTEMS™) on a 0.01 mm PET film, the SEMA pattern is transferred from the cut PET film onto the SEBS substrate with conductive paste (Dupont ™Intexar™PE874, a high recovery stretchable silver conductor). The shaped silver paste is dried at 130 °C for 15 minutes in a well-ventilated oven. A separate screen printing process is designed that consists of an upper part and a lower part to prevent potential cross-links of individual wires inside

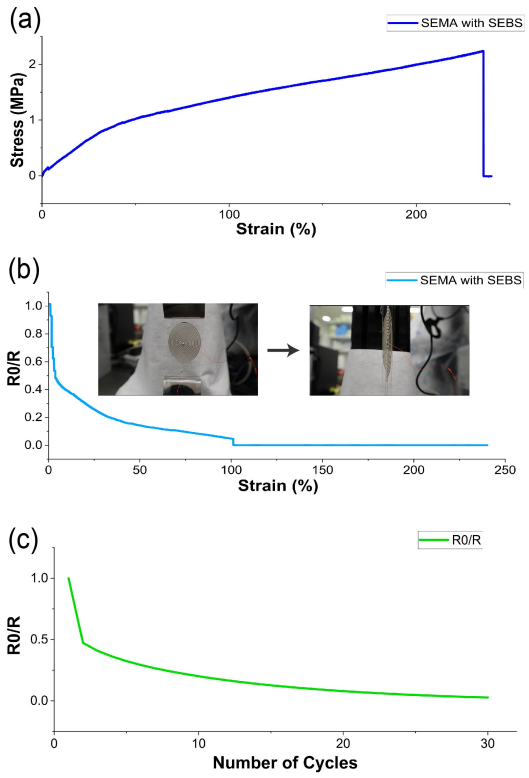

Fig. 6. Mechanical property illustrating the stretchability of the SEMA and the change in conductivity during the stretch. (a). The stress vs. strain curve. (b). The R0/R vs. strain curve. (c). The R0/R during multiple stretching cycles with a deformation of 100%.

the SEMA. A thin copper wire is then soldered to both the center and the end of the SEMA to connect the actuator to an external power.

B. Size, Shape and Heating Optimization

Changing different shapes of the SEMA seems straightforward. In theory, according to equation (1), augmenting the voltage input should proportionally escalate the magnetic force due to an increase in the current I courses through the SEMA. However, one of the major problems is the heat power generated by the SEMA. The heat power which is characterized by $P_{heat} = I^2R$, is non-uniformly distributed across the whole SEMA due to a non-uniform distribution of thickness and angles. In cases when the SEMA is designed in a square shape like in Guo et al.'s work [20] and Fig 4(b), the edges of the square result in a significantly stronger heat, resulting in the burnt of the circuit.

To investigate the optimal balance between the size and the shape of the SEMA, we designed various shapes of SEMAs with different lengths and measured their magnetic field generated at the center. The magnetic field is measured by a hand-held Gauss meter (TD8620). As shown in Fig. 5(a), there is a positive correlation between the amount of magnetic field generated and the driving voltage (as well as the current), as suggested in both measurement and equations 2 and 3. A corresponding heatmap is calculated to find the optimized construction of the SEMA size. Smaller designs

with shorter radii are favorable for their lower resistance and higher current passing through. However, this also means a higher energy generated, which generates heat that burns the circuit. Therefore, as suggested in the calculation, SEMA with a radius of 2.5 cm can generate up to 1.4 mT magnetic fields without burning, resulting in an efficient balance between reliability and the greater magnetic field generated.

We also evaluate the mechanical properties of the SEMA, showing a high mechanical compliance upon stretching. The calculated Young's Modulus (E) is approximately 2.50 MPa as well as an ultimate tensile strength (UTS) of approximately 2.24 MPa. This is feasible because of the excellent stretchability of SEBS. The conductivity shows a decreasing trend and drops to 0 at around 100% of strain (which is caused by the break in the solder point), and retains conductivity after 30 cycles of stretch.

C. Fabrication of Four-leg Under-water Soft Robot

The proof-of-concept underwater soft robot is formed by four legs and the main body, where each leg consists of one of the SEMA discussed in the previous section. The shape of the substrate is slightly adjusted to form the leg of the soft robot by replacing the glass slide with different sizes. The main body is prepared by dropping 5mL of SEBS solution into a plastic cap and waiting for the standard drying process. Finally, a 1:1 ratio of part A and part B of Ecoflex™ is used to encapsulate the silver paste as well as stick the four legs onto the main body. As the heating problem is resolved underwater, a smaller design of SEMA (1.5 cm) is applied to achieve both a stronger magnetic field it generates and a smaller leg size.

V. Results

A. Actuation Experiment

Understanding the relationship between the size of the SEMAs, the magnetic field they generate, and the force upon interacting with the permanent magnet is crucial for the design of the actuator. Besides from simulation results, we also relied on empirical experimental methods to evaluate different methods of actuation and conducted a series of experiments by placing the permanent magnet in different places relative to the SEMAs. Detailed experiments were recorded and analyzed with Tracker.

As shown in Fig. 7, a permanent magnet is placed in proximity to the SEMA at different places. The SEMA is powered by a signal generator(SIGLENT SDG 1032X Waveform Generator) with various driving voltages. When placed 2 cm parallel to the SEMA, the permanent magnet generates a homogeneous magnetic field of strength of around 100 mT perpendicular to the SEMA. When placed below the SEMA, the magnetic field is generated upward and is placed closer to the bottom to compensate for the non-homogeneity caused by varying distance to the permanent magnet.

The result indicates that when the actuator is driven by the mechanism discussed in Fig. 2(c), it results in a greater angle (a maximum of $\approx 40°$) compared to the mechanism discussed in Fig. 2(b) (a maximum of $\approx 10°$). As depicted in

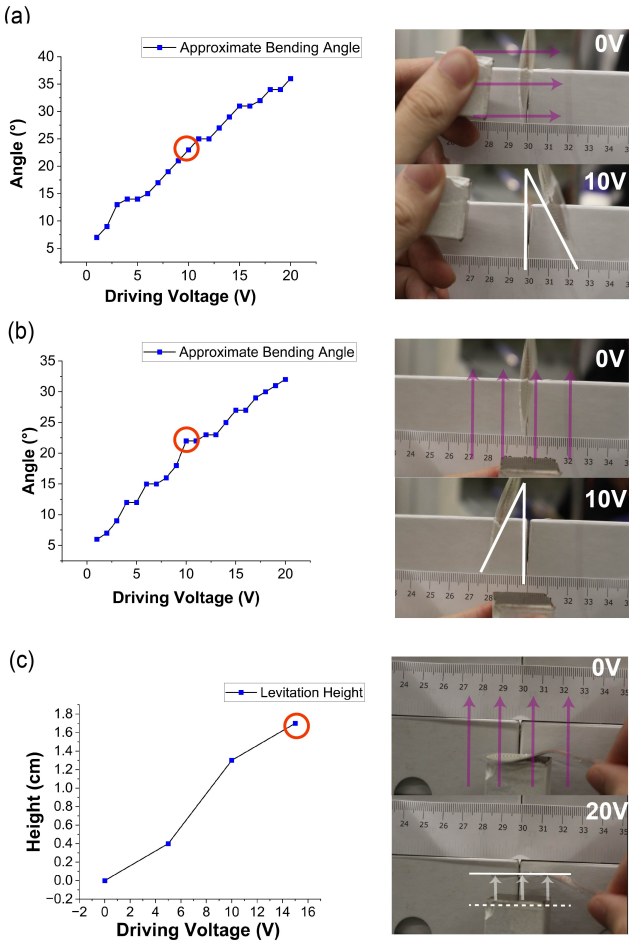

Fig. 7. The actuation experiment with different positions of permanent magnet relative to SEMA. (a). Relationship between driving voltage and bending angle when the permanent magnet is placed beside the SEMA (b). Relationship between driving voltage and bending angle when the permanent magnet is placed beside the SEMA (c). Evaluation of the elevation when the permanent magnet is placed below the SEMA

Fig 2, this is because of the existence of a self-contradictory traction force in the second mechanism. Since the direction of the flow of the electron is, relative to the permanent magnet below, opposite on the upper side and down the size of the SEMA, the upper side and the downside result in an opposite direction of traction force as well. The traction force on the lower side has a longer lever arm, resulting in a greater torque as compared to the upper side's opposite traction force. Moreover. we were also able to show a complete levitation of SEMA under the magnetic field with a driving voltage of 20V.

B. Maneuver of Soft Robot Underwater

To demonstrate the capability of the proposed SEMA as an actuator in real-world robot propulsion, a proof-of-concept underwater soft robot is built according to the method mentioned in the previous paragraph, and its behavior in underwater motion is studied in this section.

Inspired by the shape of an octopus, the underwater soft robot is composed of four legs, each load with one tethered

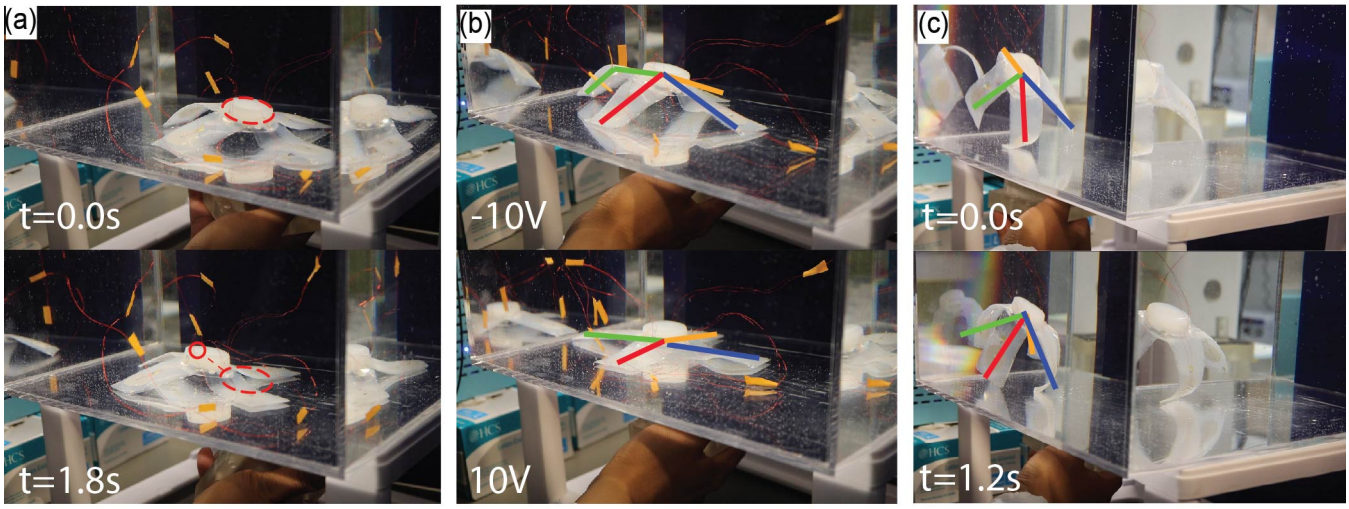

Fig. 8. Different movements performed by the proof-of-concept underwater soft robot design driven by four SEMAs. (a). An illustration showing a horizontal movement upon a manual maneuver of the permanent magnet. (b). Crawling motions performed by the soft robot when powered by an alternating current of 20 V. (c). Rotation performed by the soft robot upon floating in the middle of the water tank, driven by both the Lorentz force and the repulsive/attractive force from magnetic pole SEMA generated.

SEMA that is powered by a 20 V external power from the signal generator. As illustrated in Fig. 8, with the presence of an external permanent magnet (around 323 mT), the soft robot shows an almost infinite degree of freedom of movement underwater, including crawling, rotation, and basic up-and-down movement. Both working principles discussed in section II are utilized when performing various actions underwater.

One of the key advantages when powering the SEMA underwater is that the problem of heating, as discussed in the working principle part, is greatly eased by the high heat capacity of water. The thin property of the SEMA makes it easier for the power to dissipate. This enables a further minimized design of the SEMA as well as a higher tolerant driving voltage, which ultimately results in a greater magnetic force generated. Such an advantage is offered only when we are able to make the SEMA thin enough and is not seen in similar methods.

Note that despite the current system being tethered, our experiment showed great potential in integrating a voltage boost amplifier and making the whole system untethered. Commercially available boost converter only weighs around 5 g which is minimal compared to the weight of our soft robot, and could used to amplify a 3.3 V power source to up to 100 V, which largely exceeds the voltage usage of this experiment (20 V).

VI. DISCUSSION AND FUTURE WORK

In this work, we fabricated and analyzed our proposed SEMAS, built illustrative applications, and measured their performance underwater. The proposed fabrication technique achieved a reliable production of the SEMAS that can generate enough thrust force to drive a 16.7g soft robot underwater with a significantly low voltage (up to 20V), as compared to a common operating voltage of dielectric elastomers (up to 2kV). Our tethered underwater soft robot, as compared to other literature works, achieved a relatively higher degree of autonomy[19], [20].

Mechanically, our design excels in its flexibility and stretchability, with each individual SEMA weighing less than 0.2g and less than 0.25mm in thickness, which allows them to achieve wireless-controlled movement underwater with a high degree of freedom or to be operated in proximity to humans.

One of the key limitations of our current robot is the need for manual manipulation of an external magnetic field by handling the permanent magnet. Yet, our result indicates the potential for further scalability to a fully programmed, automated, and much stronger external magnetic field. To put this into perspective, our actuator operates within a magnetic field of approximately 300mT, dwarfed by the 7T capacity of commercial MRI machines like the MAGNETOM Terra from SIEMENS. Moreover, though the current system is tethered, the feasibility of building a completely untethered system has been proven, since the driving voltage used in the experiments can be easily achieved with any commercial boost converters. Besides, granted by the scalable nature of the fabrication process, in the future, this work can be translated to SEMAs that are extremely small for further development in terms of microrobots for tasks including the removal of blood clots, or scaling up to encompass the creation substantially greater thrust force to drive larger object.

ACKNOWLEDGMENT

This project was supported by the National Science Foundation grants 2323917, 2334134, 2216131, 2318057 (to J.L.), and the 2023 HFH+MSU Health Sciences Pilot Award (to J.L.).

REFERENCES

[1] G. Li et al., "Self-powered soft robot in the Mariana Trench," Nature, vol. 591, no. 7848, pp. 66–71, 2021.

[2] S. Kim, C. Laschi, and B. Trimmer, "Soft robotics: a bioinspired evolution in robotics," Trends in Biotechnology, vol. 31, no. 5, pp. 287–294, 2013.

[3] M. Wehner, R. L. Truby, D. J. Fitzgerald, B. Mosadegh, G. M. Whitesides, J. A. Lewis, et al., "An integrated design and fabrication strategy for entirely soft autonomous robots", Nature, vol. 536, no. 7617, pp. 451-455, 2016.

[4] M. Calisti, G. Picardi, and C. Laschi, "Fundamentals of Soft Robot locomotion," Journal of The Royal Society Interface, vol. 14, no. 130, p. 20170101, 2017.

[5] M. Duduta, D. R. Clarke, and R. J. Wood, "A high-speed soft robot based on dielectric elastomer actuators," 2017 IEEE International Conference on Robotics and Automation (ICRA), 2017.

[6] R. H. Baughman et al., "Carbon Nanotube Actuators," Science, vol. 284, no. 5418, pp. 1340–1344, 1999. doi:10.1126/science.284.5418.1340

[7] R. K. Katzschmann, A. D. Marchese, and D. Rus, "Hydraulic Autonomous Soft robotic fish for 3D swimming," Experimental Robotics, pp. 405–420, 2015.

[8] K. Tahara et al., "Rotational Angle Control of a twisted polymeric fiber actuator by an estimated temperature feedback," IEEE Robotics and Automation Letters, vol. 4, no. 3, pp. 2447–2454, 2019. doi:10.1109/lra.2019.2901982

[9] M. T. Tolley et al., "A resilient, untethered soft robot," Soft Robotics, vol. 1, no. 3, pp. 213–223, 2014. doi:10.1089/soro.2014.0008

[10] T. N. Do, H. Phan, T. Nguyen, and Y. Visell, "Miniature soft electromagnetic actuators for robotic applications," Advanced Functional Materials, vol. 28, no. 18, p. 1800244, 2018.

[11] J. Yunas et al., "Polymer-based MEMS electromagnetic actuator for Biomedical Application: A Review," Polymers, vol. 12, no. 5, p. 1184, 2020.

[12] P. Polygerinos, Z. Wang, K. C. Galloway, R. J. Wood, and C. J. Walsh, "Soft robotic glove for combined assistance and at-home rehabilitation," Robotics and Autonomous Systems, vol. 73, pp. 135–143, 2015.

[13] K. C. Galloway, K. P. Becker, B. Phillips, J. Kirby, S. Licht, D. Tchernov, et al., "Soft robotic grippers for biological sampling on deep reefs", Soft robotics, vol. 3, no. 1, pp. 23-33, 2016.

[14] T. Li et al., "Fast-moving soft electronic fish," Science Advances, vol. 3, no. 4, 2017. doi:10.1126/sciadv.1602045

[15] M. Duduta et al., "Tunable multi-modal locomotion in soft dielectric Elastomer Robots," IEEE Robotics and Automation Letters, vol. 5, no. 3, pp. 3868–3875, 2020.

[16] F. Berlinger et al., "A modular dielectric elastomer actuator to drive Miniature Autonomous underwater vehicles," 2018 IEEE International Conference on Robotics and Automation (ICRA), 2018.

[17] M. Duduta, D. R. Clarke, and R. J. Wood, "A high speed soft robot based on dielectric elastomer actuators," 2017 IEEE International Conference on Robotics and Automation (ICRA), 2017.

[18] W. Hu, G. Z. Lum, M. Mastrangeli, and M. Sitti, "Small-scale soft-bodied robot with multimodal locomotion," Nature, vol. 554, no. 7690, pp. 81–85, 2018. doi:10.1038/nature25443

[19] Y. Kim, G. A. Parada, S. Liu, and X. Zhao, "Ferromagnetic soft continuum robots," Science Robotics, vol. 4, no. 33, 2019.

[20] G. Mao et al., "Soft electromagnetic actuators," Science Advances, vol. 6, no. 26, 2020.

[21] R. Guo, L. Sheng, H. Gong, and J. Liu, "Liquid metal spiral coil enabled soft electromagnetic actuator," Science China Technological Sciences, vol. 61, no. 4, pp. 516–521, 2017.

[22] K. H. Kim and S. S. Yang, "Fabrication and test of an electromagnetic micro actuator with a planar coil on a parylene diaphragm," Micro-Electro-Mechanical Systems (MEMS), 2000.

[23] Y. Wang et al., "A micro electromagnetic actuator with high force density," Sensors and Actuators A: Physical, vol. 331, p. 112771, 2021.

[24] J. A. Roll, B. Cheng, and X. Deng, "An electromagnetic actuator for high-frequency flapping-wing Microair vehicles," IEEE Transactions on Robotics, vol. 31, no. 2, pp. 400–414, 2015.

[25] A. Foggia, E. Olivier, F. Chappuis, and J. C. Sabonnadiere, "A new three degrees of Freedom Electromagnetic Actuator," Conference Record of the 1988 IEEE Industry Applications Society Annual Meeting.

[26] G. Cahn et al., "The role of strain localization on the electrical behavior of flexible and stretchable screen printed silver inks on polymer substrates," Materialia, vol. 10, p. 100642, 2020.

[27] Q. Xu, Q. Hu, H. Wang, Z.-H. Mao, and M. Sun, "Optimal design of planar spiral coil for uniform magnetic field to wirelessly power position-free targets," IEEE Transactions on Magnetics, vol. 57, no. 2, pp. 1–9, 2021.

[28] X. Ni et al., "Soft shape-programmable surfaces by fast electromagnetic actuation of Liquid Metal Networks," Nature Communications, vol. 13, no. 1, 2022. doi:10.1038/s41467-022-31092-y

[29] Luo, Yifei, et al. "Technology roadmap for flexible sensors." *ACS nano* 17.6 (2023): 5211-5295.

[30] J. Li *et al.*, "A tissue-like neurotransmitter sensor for the brain and gut," *Nature*, vol. 606, no. 7912, pp. 94–101, 2022.

[31] S. Niu *et al.*, "A wireless body area sensor network based on stretchable passive tags," *Nature Electronics*, vol. 2, no. 8, pp. 361–368, 2019. doi:10.1038/s41928-019-0286-2